31.0 ACCUMULATIVE ROLL BONDING OF AL AND TI SHEETS TOWARD LOW TEMPERATURE SUPERPLASTICITY

Brady McBride (Mines)
Faculty: Kester Clarke (Mines)
Industrial Mentor: Ravi Verma (Boeing) and John Carpenter (LANL)

This project initiated in Fall 2017. The research performed during this project will serve as the basis for a Ph.D. thesis program for Brady McBride.

31.1 Project Overview and Industrial Relevance

Accumulative roll bonding (ARB) is a severe plastic deformation technique used to produce ultra-fine-grained material by introducing large plastic strains [31.1]. The surfaces of two sheets are commonly wire-brushed before being stacked and roll bonded together in a conventional rolling mill [31.1]. After rolling, the material is sectioned in half and the process is repeated. A single-pass, 50% rolling reduction is commonly employed to ensure adequate bonding and to retain the original dimensions after each cycle [31.1]. The ARB process is largely different from conventional rolling processes in that heavy, unlubricated, single-pass reductions are used. This imparts redundant shear into the surface of the rolled material which is introduced through thickness with subsequent roll bonding cycles [31.2]. The combination of redundant shear and large rolling reductions ultimately lead to grain refinement.

The attraction to ARB lies in the ability to produce ultra-fine-grained material with conventional processing equipment while maintaining consistent sample geometry. With the accumulation of large strains, dislocation cell structures form within the material that further develop into refined grains [31.3, 31.4]. Ultra-fine grains (~250 nm) produced after 5 cycles of ARB in Al 5083 have exhibited tensile elongations in excess of 200% for strain rates of 10^{-3} s^{-1} at 200 °C [31.5]. In comparison, superplastic deformation of Al 5083 produced with conventional processing methods typically requires temperatures of 500 °C and strain rates above 10^{-3} s^{-1} to produce elongations around 300%. Enhanced superplasticity provided by the ARB process would be beneficial to superplastic sheet forming operations where reduced temperatures and/or increased strain rates could lead to cost savings and reduced die wear. Additionally, ARB processing may produce sheets that retain a fine grain structure after forming operations.

31.2 Previous Work – Mitigation of Edge Cracking with Artificial Constraint

One of the limitations of ARB is the development of edge cracking, which generally occurs as a result of material overhang, lateral spreading or a combination of both. Material overhang cracking occurs due to poor sheet alignment as the material enters the mill; this can be mitigated by wire binding the sheets to restrict movement during rolling. Edge cracking due to lateral spreading is commonly reported in literature [31.1,31.4], but mitigation strategies have not been presented in much detail. In previous work for this project [31.6], it was found that roll bonding strips within a frame of sacrificial material made of easily deformable Al 1100 imposes sufficient lateral constraint to reduce lateral spreading. Sacrificial frame widths with 6 mm of constraint were found to maximize the trade-off between providing adequate constraint without increasing rolling loads [31.6]. This technique was applied to 5 consecutive cycles of ARB and reduced lateral spreading by up to 50 % for reach roll bonding cycle. This processing technique reduced the amount of edge material that had to be removed by shearing and ultimately improved sample yield. The time spent in optimizing a roll bonding process will aid in mass sample production for the remainder of this project.

31.3 Recent Progress

31.3.1 Characterization of Grain Refinement through ARB Processing

The ARB processing pathway leads to development of an ultra-fine-grained structure in two ways. First, redundant shear occurs at the sample surface due to the large, unlubricated rolling reduction. Secondly, the subsequent roll bonding pass introduces this heavily sheared region into the mid-thickness of the sample. With each additional roll bonding pass, the original heavily sheared region is introduced in the quarter-thickness, semi-quarter-thickness, and so on, until the sheared regions are distributed through thickness.

ARB studies are commonly conducted with 5 or 6 sequential roll-bonding cycles, corresponding to equivalent strains of 4 to 4.8, at which point hardness, yield strength and ultimate tensile strength approach saturation [31.4]. By investigating grain size and grain boundary character via electron backscatter diffraction (EBSD), studies on interstitial-free steel have shown high angle grain boundary (HAGB) percentages and subgrain size to stabilize after 5 cycles, concurrent with a relatively homogenous microstructure through thickness [31.7].

In order to confirm 5 cycles of ARB is sufficient in creating a relatively homogenous microstructure, a similar study to that conducted on interstitial-free steel [31.7] was conducted on Al 5083. Samples were prepared with up to 5 cycles of ARB by preheating for 5 minutes in an air furnace at 250 °C and roll bonding with single, 50% unlubricated rolling reductions. The use of wire binding and artificial constraint as described above were applied to mitigate edge cracking. EBSD scans were conducted on the RD-ND plane near the surface of the sheet, in the vicinity of the bond formed during the first ARB cycle, and at the centerline bond location. Examination near the first bond was chosen for analysis as this is the region through the sample thickness that exhibits the least amount of shear strain as modeled by Kamikawa [31.7]; this region is likely to be the least refined and will serve as an indicator of homogenous microstructural refinement.

Table 31.1 shows inverse pole figure (IPF) maps obtained from this study with a grain boundary misorientation map superimposed. The microstructure of early ARB cycles is characterized by relatively large grains containing many low angle grain boundaries (LAGBs). After the third cycle, low aspect ratio grains characterized by HAGBs start to form at the sheet surface, while grains remain elongated and substructured in the sheet interior. After the fifth cycle, grains consist of HAGBs through thickness, but remain elongated in the vicinity of the first bond and at the centerline. The change in grain boundary character, from LAGBs to HAGBs, is summarized in **Figure 31.1**, where it is shown that a saturation in HAGBs is approached after 5 ARB cycles.

The IPF maps in **Table 31.1** show the grain structure after 5 ARB cycles consists of 250 nm by 1 μm grains elongated in the rolling direction. Near the surface of the sheet, grains are more equiaxed with a diameter of roughly 250 nm. These results are in agreement with other studies [31.5], which characterized grains as being equiaxed and roughly 250 nm as seen via TEM in the RD-TD plane. For this project it has been decided to maintain a constant processing path (5 ARB cycles, 5 min preheats at 250 °C with 50% unlubricated rolling reductions) for samples to limit the number of experimental degrees of freedom. Thus, this characterization of 5 cycle ARBed material, as shown in this section, serves as the microstructural baseline for the remainder of this project.

31.3.2 Microstructural Analysis After Preliminary Superplastic Tensile Testing

Previous work on this project consisted of preliminary testing of both ARBed and conventionally processed Al 5083 specimens for superplasticity. The as-tested specimens and total elongations for tests conducted at a variety of temperatures with an initial strain rate of 10^{-3} s^{-1} are shown in **Figure 31.2**. All tests had a 5 min preheat time prior to the start of the tensile test. The ARBed specimens exhibited higher tensile elongations and more diffuse necking than the conventionally processed samples.

IPF maps were created from EBSD scans on areas in both the grip and gauge sections of the ARBed material after tensile deformation. The gauge section represents microstructural changes during elevated temperature tensile testing at an initial strain rate of 10^{-3} s^{-1}. The grip sections represent microstructural changes after a static anneal, where the duration of the anneal was determined by time taken for the gauge section to strain to failure. These results are summarized in **Table 31.2**. Static annealing at 196 °C (30 min) and 290 °C (37 min) lead to a more equiaxed microstructure than immediately after 5 ARB cycles. Furthermore, static annealing at 196 °C created a banded microstructure with grains on the order of 500 nm, whereas static annealing at 290 °C lead to a bimodal grain size distribution with grain sizes between 1 and 10 μm. At 377 °C (69 min), grain growth is evident with elongated grains roughly on the scale of 5 to 15 μm.

After elevated temperature testing at 196 and 290 °C the grains appear relatively equiaxed and retain grain sizes under 2 μm. This microstructure is highly conducive for grain boundary sliding and is likely to be accompanied with a weakening in texture [31.8]. At 377 °C, the grains are elongated in the tensile direction, which suggests diffusional creep as a primary deformation mechanism [31.8]. From this preliminary data it can be hypothesized that grain size remains relatively stable during elevated temperature deformation for temperatures as high as 300 °C and an initial strain rate of 10^{-3} s^{-1}.

Characterization of failure mechanisms (i.e. diffuse vs localized necking) and void formation are two other important aspects of superplasticity testing. **Figure 31.3** shows backscatter electron images taken at the through-thickness centerline after failure of the three samples mentioned above. Area fractions of voids have been calculated and are displayed as figure insets. The void formation for samples tested below 300 °C are circular in nature and are randomly dispersed through the microstructure, whereas above 300 °C, voids appear to nucleate, grow and coalesce preferentially along discontinuities such as bonding interfaces and second phases. These observations suggest void formation and growth is largely dependent on the dominant deformation mechanism during tensile testing.

Work to date has shown there are multiple competing factors at play when optimizing superplasticity, including maximizing tensile elongation, retaining a fine-grain structure and minimizing void formation. An understanding of dominant deformation mechanisms during superplastic deformation will aid in optimizing the superplastic response of ARBed Al 5083. The primary scope of this project moving forward will be to identify the primary deformation mechanisms that are active and investigate how microstructures can be altered (i.e. through static annealing or prestraining) to optimize combinations of these conflicting parameters.

31.4 Plans for Next Reporting Period

Iterative testing phases will be conducted for the remainder of this project to identify optimal parameters for superplasticity in ARBed Al 5083. A comprehensive first round of tensile testing will be conducted to have an understanding of temperature and strain rate ranges of interest. After microstructural characterization and a strain rate sensitivity analysis, another, in-depth round of tensile testing will be conducted to optimize the superplastic response of this material. For the next reporting period, the following actions will be pursued:

- Bulk production of samples processed with 5 ARB cycles to satisfy future testing needs
- Comprehensive static annealing trials to help inform temperature range for first round of tensile testing
- First-round of comprehensive tensile tests (200 – 400 °C**,** 10^{-2} to 10^{-4} s^{-1}) to serve as a basis for future testing aimed at optimizing microstructures for superplasticity
- Production of larger-scale samples, as access to collaborative high-capacity rolling equipment permits, to investigate other areas such as anisotropy and formability testing
- PhD Thesis Proposal formally outlining the scope, intent and objectives of this project

31.5 References

[31.1] Y. Saito, H. Utsunomiya, N. Tsuji, T. Sakai, Novel Ultra-High Straining Process For Bulk Materials - Development of the Accumulative Roll Bonding (ARB) Process, Acta Materialia. 47 (1999) 579–583.

[31.2] S.H. Lee, Y. Saito, N. Tsuji, H. Utsunomiya, T. Sakai, Role of shear strain in ultragrain refinement by accumulative roll-bonding (ARB) process, Scripta Materialia. 46 (2002) 281–285.

[31.3] Y. Saito, N. Tsuji, H. Utsunomiya, T. Sakai, R. Hong, Ultra-fine grained bulk aluminum produced by accumulative roll-bonding (ARB) process, Scripta Materialia. 40 (1999) 795–800.

[31.4] M. Reza, F. Ashrafizadeh, R. Jamaati, On the use of accumulative roll bonding process to develop nanostructured aluminum alloy 5083, Materials Science & Engineering A. 561 (2013) 145–151.

[31.5] N. Tsuji, K. Shiotsuki, Y. Saito, Superplasticity of Ultra-Fine Grained Al-Mg Alloy by Accumulative Roll Bonding, Mater. Trans. 40 (1999) 765–771.

[31.6] B. McBride, A.J. Clarke, and K.D. Clarke, "Mitigation of Edge Cracking during Accumulative Roll Bonding (ARB) of Aluminum Alloys" North American Deep Drawing Research Group (NADDRG) Fall 2019 meeting, November 2019, Plymouth, MI.

[31.7] N. Kamikawa, T. Sakai, N. Tsuji, Effect of redundant shear strain on microstructure and texture evolution during accumulative roll-bonding in ultralow carbon IF steel, Acta Materialia 55 (2007) 5873-5888.

[31.8] J. Pilling & N. Ridley, Superplasticity in Crystalline Solids, The Institute of Metals, London.

31.6 Figures and Tables

Table 31.1: Electron backscatter diffraction (EBSD) inverse pole figure (IPF) maps showing grain refinement after sequential ARB cycles in the RD-ND plane. EBSD scans were conducted 10 µm from the sample surface, in the vicinity of the first ARB bond and at the centerline of each sheet.

	10 µm from Surface	First Bond	Centerline Bond
1 ARB Cycle	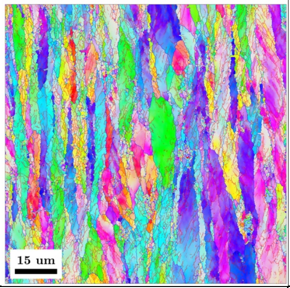	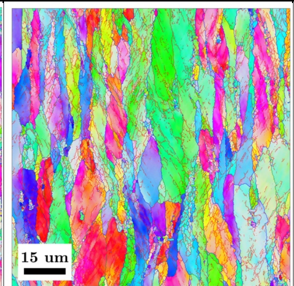	For 1 ARB cycle, the first bond is the same as the centerline bond.
2 ARB Cycles	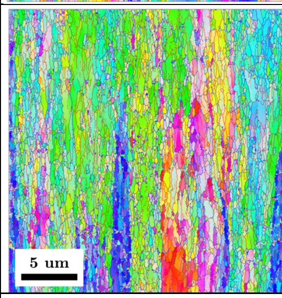	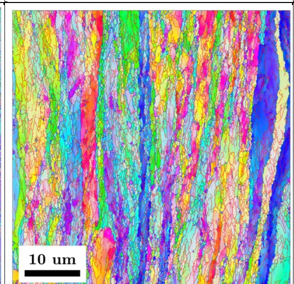	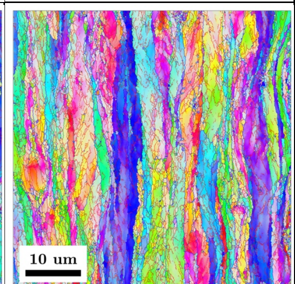
3 ARB Cycles	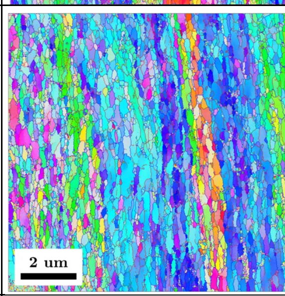	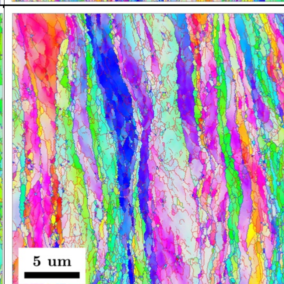	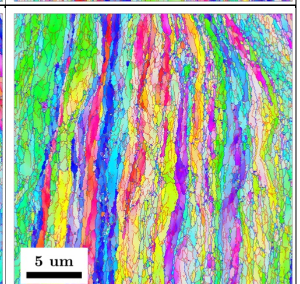
4 ARB Cycles	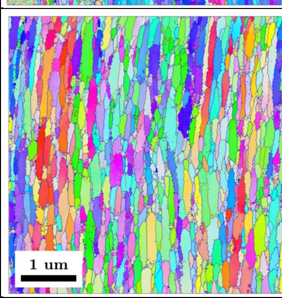	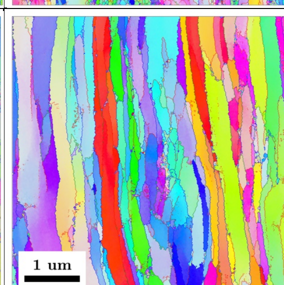	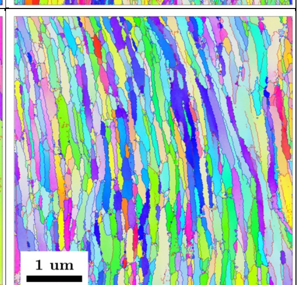
5 ARB Cycles 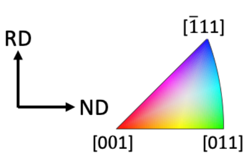	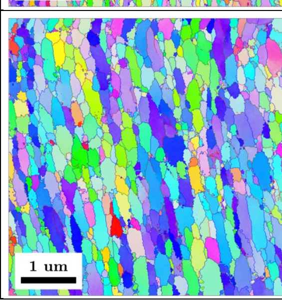	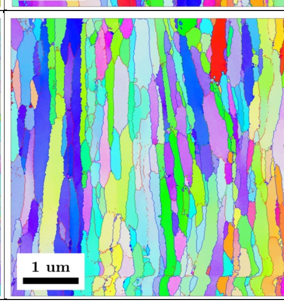	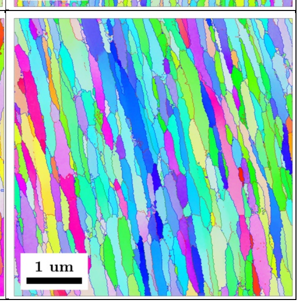

Table 31.2: EBSD inverse pole figure maps obtained from grip and gauge sections of tensile specimens after testing for superplasticity. The grip section represents a static anneal, with length of anneal based on time taken to strain to failure. Note that the rolling direction is parallel to the tensile axis.

	196 °C (30 min)	**290 °C (37 min)**	**277 °C (69 min)**
Gauge Section	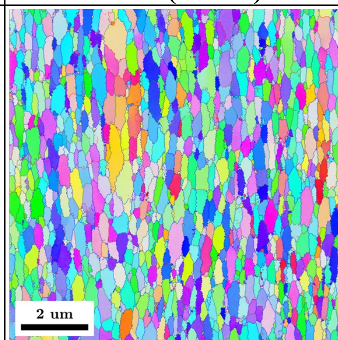	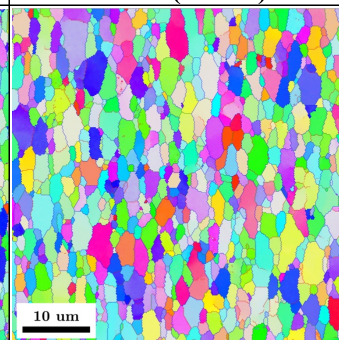	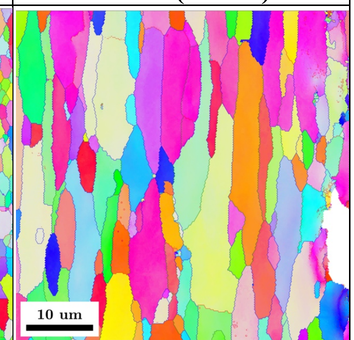
Grip Section (static anneal) 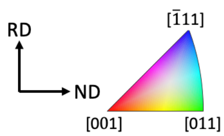	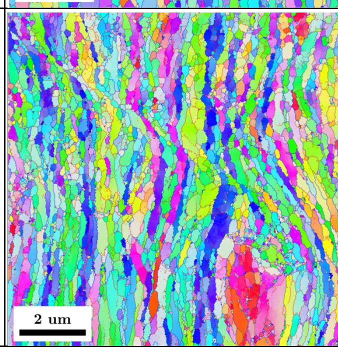	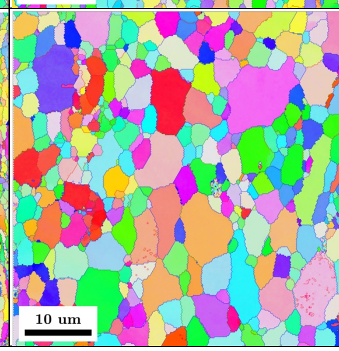	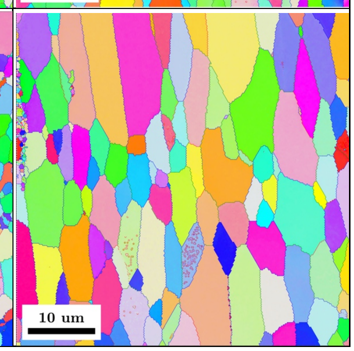

.

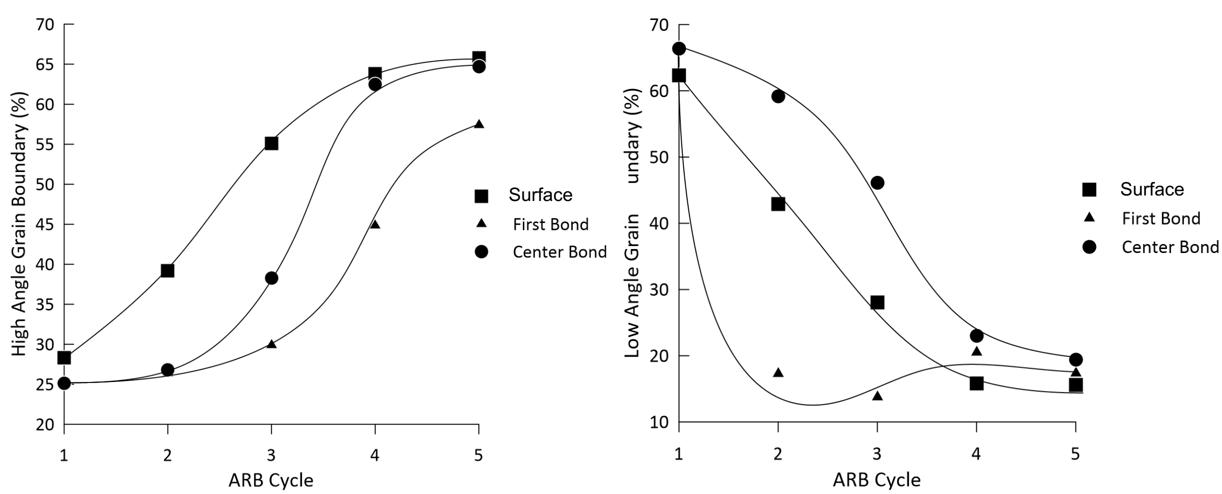

Figure 31.1: High angle grain boundary (HAGB) and low angle grain boundary (LAGB) fractions for Al 5083 processed through 5 ARB cycles. Measurements were obtained through electron backscatter diffraction (EBSD) misorientation data as presented in Table 1. LAGBs are defined as misorientations between 2° and 15°; HAGB are defined as misorientations greater than 30°. As the transition from LAGB to HAGB is diffuse, intermediate angle grain boundaries (IAGB), those that have misorientations between 15 and 30°, have been excluded.

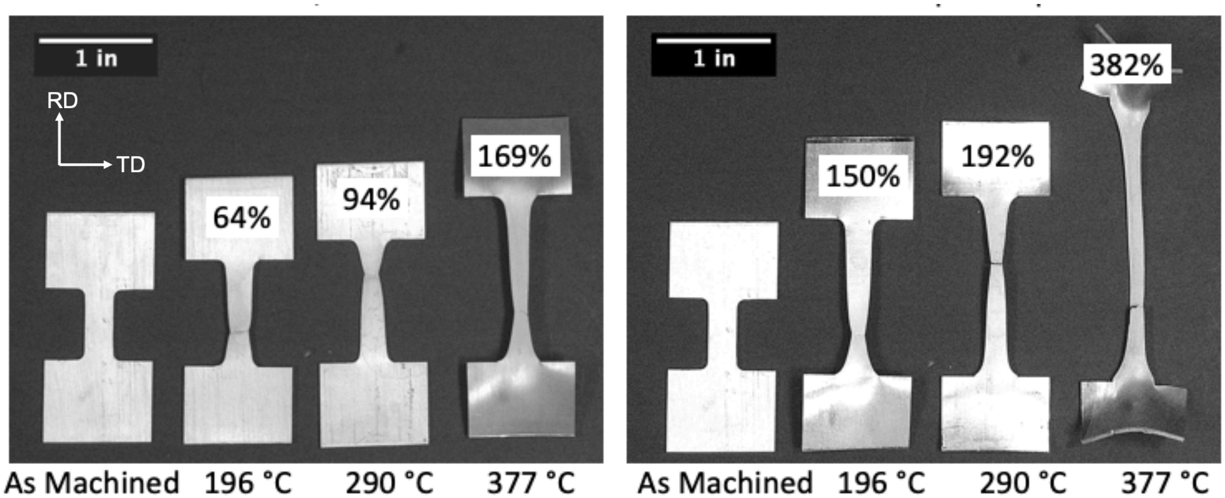

(a) (b)

Figure 31.2: Tensile specimens after elevated temperature testing for superplasticity with initial strain rate of 10^{-3} s^{-1}, operating with constant crosshead displacement. Subfigure (a) shows conventionally recrystallized Al 5083 with ~15 µm grain size while subfigure (b) shows 5-cycle ARBed Al 5083 with ~250 nm x 1 µm x 1 µm grain size. Note temperatures shown are those measured at the gauge section for a given furnace setpoint; stringent calibration of the furnace zones has since been implemented to test at more "round" temperatures in the future. Also note a prototype superplastic grip design was used for these tests, which lead to noticeable distortion of the 377 °C samples in the grip regions; a new grip design has since been created to alleviate this issue.

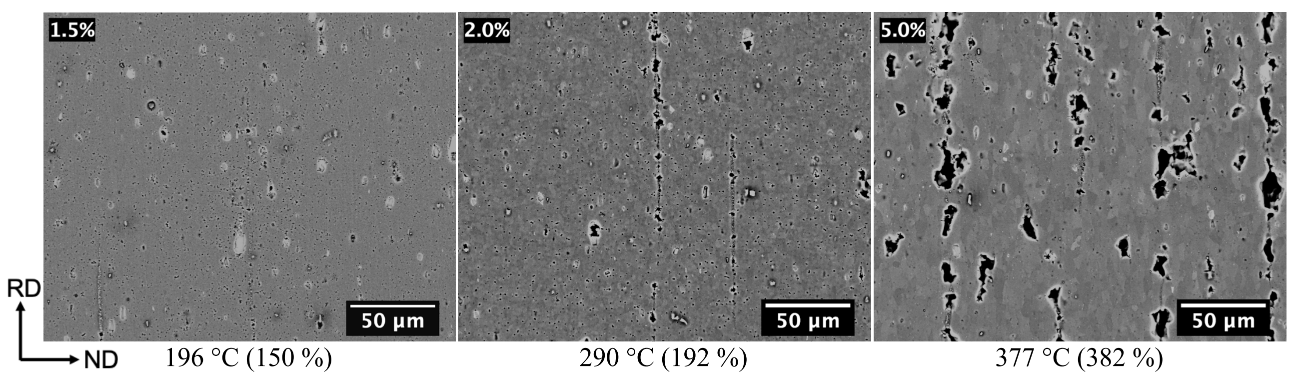

196 °C (150 %) 290 °C (192 %) 377 °C (382 %)

Figure 31.3: Backscatter electron images showing void formation at the through-thickness centerline of the gauge section after tensile testing for superplasticity at an initial strain rate of 10^{-3} s^{-1}. Note the tensile axis is parallel to the rolling direction. The void fraction is shown inset in each image, calculated by thresholding in ImageJ. The elongation to failure and tensile testing temperature for each sample is recorded below each image.